Improving the acousto-optical interaction in a Mach-Zehnder interferometer

Dühring, Maria Bayard; Sigmund, Ole

Published in:
Journal of Applied Physics

Link to article, DOI:
10.1063/1.3114552

Publication date:
2009

Document Version
Publisher's PDF, also known as Version of record

Improving the acousto-optical interaction in a Mach–Zehnder interferometer

Maria B. Dühring[a] and Ole Sigmund
Department of Mechanical Engineering, Solid Mechanics, Technical University of Denmark, 2800 Lyngby, Denmark

(Received 2 December 2008; accepted 1 March 2009; published online 22 April 2009)

A method for modeling the interaction of the mechanical field from a surface acoustic wave and the optical field in the waveguides of a Mach–Zehnder interferometer is presented. The surface acoustic wave is generated by an interdigital transducer using a linear elastic plane model of a piezoelectric, inhomogeneous material, and reflections from the boundaries are avoided by applying perfectly matched layers. The optical modes in the waveguides are modeled by time-harmonic wave equations for the magnetic field. The two models are coupled using stress-optical relations and the change in effective refractive index introduced in the Mach–Zehnder interferometer arms by the stresses from the surface acoustic wave is calculated. It is then shown that the effective refractive index of the fundamental optical mode increases at a surface acoustic wave crest and decreases at a trough. The height and the width of the waveguides are varied for a silicon on insulator sample, and it is shown that the difference in effective refractive index between the waveguides can be increased 12 times for the right choice of waveguide size such that the optical modulation is improved. The difference is four times bigger if the waveguides are kept single moded. It is furthermore shown that the difference increases more than ten times when the waveguides are buried below the surface, where the mechanical stresses have their maximum, and in the case where two interdigital transducers are used the difference is increased 1.5 times. © *2009 American Institute of Physics*. [DOI: 10.1063/1.3114552]

I. INTRODUCTION

In the last four decades, surface acoustic waves (SAWs) have received increasing attention and have found use in a range of different applications. One type of SAW, also known as a Rayleigh wave, is defined as elastic vibrations that propagate along a material surface and consists of a longitudinal and a shear component.[1] There is almost no decay of the amplitude along the propagation direction, but there is exponential decay into the bulk material such that most of the energy density is confined within one wavelength of the surface. In piezoelectric materials the elastic field is accompanied by an electric field, and in these materials it was suggested by White and Voltmer[2] in 1965 to generate SAWs by interdigital transducers (IDTs) by the inverse piezoelectric effect. Since then, SAWs have been widely used in electromechanical filters and resonators in telecommunication as well as in oscillators and sensors.[3–5] In recent years another application of SAWs has been introduced, which is modulation of optical waves for signal generation in semiconductor structures.[6,7] Experimental results are reported in Refs. 8 and 9 for a compact and monolithic modulator consisting of a SAW driven Mach–Zehnder interferometer (MZI). The relative modulation obtained with waveguides of GaAs on an AlGaAs layer and with straight IDTs exceeded 40%. However, for silicon waveguides on a silica layer, materials which are easier to work with and common in optical components, only a relative modulation between 0% and 8 % was obtained. Here a general finite element model for calculating the acousto-optical interaction between SAWs and optical waves is presented and it is employed to improve the modulation of the optical wave in the silicon on insulator (SOI) MZI. The interaction is simulated by coupling a model of a piezoelectric material with an optical model where the effective refractive indices for the propagating optical modes can be calculated by solving the in-plane time-harmonic wave equation. Finite element simulation of SAWs in a piezoelectric material has been discussed by others for both stratified, periodic structures[10,11] as well as for finite domains with straight surfaces and a single piezoelectric material.[12] In this work the periodic model presented in Ref. 11 for a piezoelectric material is used for a stratified structure and is furthermore extended to finite structures by employing perfectly matched layers (PMLs),[13] which surround the SAW device such that reflections from the domain boundaries are avoided. With this model it is possible to simulate nonperiodic SAW devices on a stratified structure. A description of the MZI problem and the coupled acousto-optical model is found in Sec. II. In Sec. III results on the SAW generation and the optical modes are presented and it is shown how the optical modulation in the MZI can be improved by changing the height and width of the waveguides and introducing other changes in the structure. Section IV concludes the article and suggests further work.

II. THE ACOUSTO-OPTICAL MODEL

A. Problem description

In this work a numerical model of SAW driven light modulation in a MZI is presented. A MZI is an optical device consisting of a ridge waveguide that is split into two waveguide arms and after a distance the arms are joined into one

[a]Electronic mail: mbd@mek.dtu.dk.

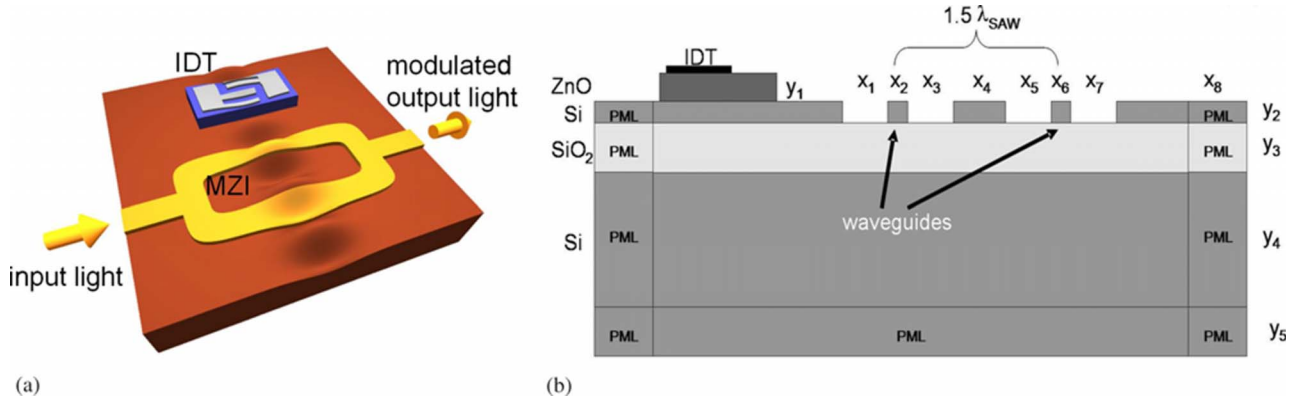

FIG. 1. (Color online) Light modulation in a MZI with a SAW generated by an IDT. (a) Three dimensional geometry of a MZI with a propagating SAW ([van der Poel (Ref. 9)]. (b) A 2D cross section through the waveguide arms of the MZI, which is used in the simulations. The SAW is absorbed in PMLs at the boundaries. The dimensions indicated in are in microns given by $x_1=2.77$, $x_2=0.45$, $x_3=2.79$, $x_4=2.39$, $x_5=2.77$, $x_6=0.45$, $x_7=2.79$, $x_8=15.0$, $y_1=0.5$, $y_2=2.34$, $y_3=1.0$, $y_4=16.8$, and $y_5=15.0$.

waveguide again as illustrated by Fig. 1(a). When a SAW is propagating perpendicular to the waveguide arms it is possible to obtain a periodic modulation of the light. When the distance between the waveguide arms is an unequal number of half SAW wavelengths, different situations will occur. At one point in time, a wave node will be present at each waveguide and the output light will not change. In another point in time, a wave crest will be located at one waveguide, whereas a trough will appear at the other waveguide. The applied stresses with opposite sign will introduce a refractive index difference in the arms, which causes an opposite phase change in them. By constructive and destructive interferences the light will be turned on and off periodically with a multiplum of the SAW frequency depending on the static phase difference in the two arms, which can be introduced by a length difference between them. To model the SAW propagation and the optical modes in the waveguides, it is sufficient to consider a two dimensional (2D) model of a cross section of the two waveguides as seen on Fig. 1(b). The SAW is generated at the IDT to the left and propagates in both the left and the right horizontal direction and is absorbed in the PMLs. To the right the SAW will pass through the two waveguides. To simulate the acousto-optical interaction in the MZI a model describing the SAW generation in a piezoelectric material is coupled with an optical model describing the propagation of the light waves in the waveguides. It is assumed that the stress-optical effect is dominant compared to the electro-optical effect, which will be neglected here (see Ref. 8). It is furthermore assumed that the SAW will affect the optical wave, but the optical wave will not influence the SAW, so the problem is solved by first calculating the stresses in the MZI introduced by the SAW. Then the change in refractive index in the materials due to the stresses can be calculated, and finally by solving the optical model the effective refractive index of the different possible light modes can be determined. The mathematical model, which is solved by the commercial finite element program COMSOL MULTIPHYSICS,[14] is described in the following subsections.

B. The piezoelectric model

The SAW is generated in a piezoelectric material by applying an electric potential to the electrode fingers of the IDT on the surface of the solid. The applied electric field will introduce mechanical displacements in the solid by the inverse piezoelectric effect. The behavior of the piezoelectric material is described by the following model as found in Ref. 15. The mechanical strain S_{ij} is for small displacements given by the tensor expression

$$S_{ij} = \frac{1}{2}\left(\frac{\partial u_i}{\partial x_j} + \frac{\partial u_j}{\partial x_i}\right), \tag{1}$$

where u_i are the displacements and x_i are the coordinates. The stresses T_{ij} have to fulfill Newton's second law for a dynamic problem. The SAW is generated by applying a harmonic electric potential V to the electrodes given by

$$V(x_j,t) = V(x_j)e^{i\omega_{\mathrm{SAW}}t}, \tag{2}$$

where ω_{SAW} is the angular frequency of the potential driving the SAW and t is the time. As the electric field is harmonic, the strain and stresses will vary harmonically as well and Newton's second law takes the form

$$\frac{\partial T_{ij}}{\partial x_j} = -\rho\omega_{\mathrm{SAW}}^2 u_i, \tag{3}$$

where ρ is the density of the material. The electrical behavior of the material is described by Maxwell's equations for the electric field. It is assumed that there are no free electric charges in the material, so Gauss' law reduces to

$$\frac{\partial D_j}{\partial x_j} = 0, \tag{4}$$

where D_j is the electric displacement. The electric field E_j can be derived from a scalar potential as in electrostatic problems, and Faraday's law then states

$$E_j = -\frac{\partial V}{\partial x_j}. \tag{5}$$

The mechanical stresses and the electric displacement both depend on the strain and the electric field by the constitutive relations

$$T_{jk} = \tilde{c}^E_{jklm} S_{lm} - \tilde{e}^T_{ijk} E_i, \tag{6}$$

$$D_i = \tilde{e}_{ijk} S_{jk} + \tilde{\varepsilon}^S_{ij} E_j, \tag{7}$$

where $\tilde{c}^E_{jklm}$ are the elastic stiffness constants, $\tilde{e}_{ijk}$ are the piezoelectric stress constants, and $\tilde{\varepsilon}^S_{ij}$ are the permittivity constants. The materials are, in general, anisotropic, and as it is only possible to generate the SAW by the inverse piezoelectric effect in certain directions, the material tensors have to be rotated. This is indicated by the tilde above the material tensors. The rotation is done according to Euler's transformation theory as explained in Ref. 16. Here the relation between the original directional vector r_j and the rotated vector $\hat{r}_i$ is given by

$$\hat{r}_i = a_{ij} r_j, \tag{8}$$

where a_{ij} is the transformation matrix given by the Euler angles φ_1, φ_2, and φ_3, where the crystal axes are rotated clockwise about the x_3-axis, then the x_2-axis, and finally the x_3-axis again. The material property matrices can then be transformed by the transformation matrix a_{ij} and the Bold matrix M_{ijmn} as follows:

$$\tilde{c}^E_{ijkl} = M_{ijmn} M_{klpq} c^E_{mnpq}, \quad \tilde{e}_{ijk} = a_{il} M_{jkmn} e_{lmn},$$

and

$$\tilde{\varepsilon}^S_{ij} = a_{ik} a_{jl} \varepsilon^S_{kl}. \tag{9}$$

At the boundaries, both mechanical and electrical conditions must be specified to solve the problem. Considering the mechanical conditions the upper surface is stress-free and the sides and the bottom are clamped outside the PMLs,

$$\text{stress free surface:} \quad T_{jk} m_k = 0, \tag{10}$$

$$\text{clamped surface:} \quad u_i = 0, \tag{11}$$

where m_k is the normal unit vector pointing out of the surface. At the upper surface there are no charges and therefore electric insulation occurs, meaning that the normal component of the electric displacement is zero. At the sides and at the bottom of the domain it is assumed that the electric potential is zero, whereas at the interface between the electrodes and the substrate the potential is V_p at the positively charged electrodes and $-V_p$ at the negatively charged electrodes. The electrical boundary conditions are summarized below,

$$\text{electric insulation:} \quad D_i m_i = 0, \tag{12}$$

$$\text{zero potential:} \quad V = 0, \tag{13}$$

$$\text{applied positive potential:} \quad V = V_p, \tag{14}$$

$$\text{applied negative potential:} \quad V = -V_p. \tag{15}$$

The piezoelectric problem is solved by a plane formulation obtained by setting S_{i3}, S_{3j} and E_3 as well as T_{i3}, T_{3j}, and D_j equal to zero. The governing equations (3) and (4) are solved simultaneously to find the three unknowns u_1, u_2, and V.

1. PMLs

To prevent reflections of the SAW from the outer boundaries, which will disturb the wave propagation, PMLs are applied around the regular domain as illustrated on Fig. 1(b). In Ref. 13 PMLs are introduced for time-harmonic elastodynamic problems and are now extended to piezoelectric materials. The PMLs have the property that the mechanical and the electrical disturbances are gradually absorbed in the layers before they reach the outer boundaries. In this way there are no reflections that can disturb the propagation of the SAW and an infinite domain is thus simulated by a finite domain. An artificial damping γ_j at position x_j in the PMLs is introduced on the form

$$\gamma_j(x_j) = 1 - i\sigma_j (x_j - x_l)^2, \tag{16}$$

where x_l is the coordinate at the interface between the regular domain and the PML and σ_j is a suitable constant. The damping is introduced in the expressions for the strain and the electric field,

$$S_{ij} = \frac{1}{2}\left(\frac{1}{\gamma_j}\frac{\partial u_i}{\partial x_j} + \frac{1}{\gamma_i}\frac{\partial u_j}{\partial x_i}\right) \quad \text{and} \quad E_j = -\frac{1}{\gamma_j}\frac{\partial V}{\partial x_j}, \tag{17}$$

as well as in the governing equations for the piezoelectric material

$$\frac{1}{\gamma_j}\frac{\partial T_{ij}}{\partial x_j} = -\rho\omega^2 u_i \quad \text{and} \quad \frac{1}{\gamma_j}\frac{\partial D_i}{\partial x_j} = 0. \tag{18}$$

There is no damping outside the PMLs and here $\gamma_j = 1$. A suitable thickness of the PMLs as well as the value of σ_j must be found by numerical experiments such that both the mechanical and electrical disturbances are absorbed before reaching the outer boundaries. However, the absorption must also be sufficiently slow as reflections will occur at the interface between the regular domain and the PML if their material properties are not comparable.

C. The optical model

After the mechanical stresses in the material have been computed by the piezoelectric model described above, the refractive index n_{ij} in the stressed material can be calculated according to the stress-optical relation[17]

$$n_{ij} = n^0_{ij} - \tilde{C}_{ijkl} T_{kl}, \tag{19}$$

where n^0_{ij} is the refractive index in the stress-free material. $\tilde{C}_{ijkl}$ are the rotated stress-optical constants obtained by the expression

TABLE I. The elastic stiffness constants (10^{11} N m^{-2}) and the density (kg m^{-3}) for the materials used in the piezoelectric model.

Material	c_{11}^E	c_{12}^E	c_{13}^E	c_{22}^E	c_{23}^E	c_{33}^E	c_{44}^E	c_{55}^E	c_{66}^E	ρ
GaAs	1.183	0.532	0.532	1.183	0.532	1.183	0.595	0.595	0.595	5316.5
Si	1.660	0.639	0.639	1.660	0.639	1.660	0.796	0.796	0.796	2330
SiO_2	0.785	0.161	0.161	0.785	0.161	0.785	0.312	0.312	0.312	2200
ZnO	2.090	1.205	1.046	2.096	1.046	2.106	0.423	0.423	0.4455	5665

$$\tilde{C}_{ijkl} = M_{ijmn} M_{klpq} C_{mnpq}. \tag{20}$$

For a given optical mode of order ν and with the out of plane propagation constant β_ν, the effective refractive index $n_{\text{eff},\nu}$ is defined as

$$n_{\text{eff},\nu} = \beta_\nu / k_0, \tag{21}$$

where k_0 is the free space propagation constant. It is assumed that the propagating optical modes have harmonic solutions on the form

$$H_{p,\nu}(x_1, x_2, x_3) = H_{p,\nu}(x_1, x_2) e^{-i\beta_\nu x_3}, \tag{22}$$

where $H_{p,\nu}$ is the magnetic field of the optical wave. The governing equation for the magnetic field is thus the time-harmonic wave equation

$$e_{ijk} \frac{\partial}{\partial x_j} \left(b_{kl} b_{lm} e_{mnp} \frac{\partial H_p}{\partial x_n} \right) - k_0^2 H_p = 0, \tag{23}$$

where e_{ijk} here is the alternating symbol and $b_{ik} n_{kj} = \delta_{ij}$. For a given value of k_0, the propagation constant β_ν for the possible modes is found by solving the wave equation as an eigenvalue problem, whereby the effective refractive indices can be obtained. In this work the set of equations are reduced such that the model is only solved for the transverse components of the magnetic fields H_1 and H_2. As the energy of the lower order optical modes is concentrated in the waveguides, the calculation domain, where the eigenvalue problem is solved, can be reduced to a smaller area around each of the waveguides. At the boundary of such a domain it is assumed that the magnetic field is zero as the energy density quickly decays outside the waveguide, thus the boundary condition is

$$e_{ijk} H_j m_k = 0, \tag{24}$$

where e_{ijk} again is the alternating symbol and m_k is the normal unit vector pointing out of the surface.

III. RESULTS

In this section results are presented for the SAW propagation, the optical waves in the waveguides, and their acousto-optical interaction.

A. Simulation of SAWs

The piezoelectric model is first employed to solve the propagation of a SAW in a GaAs sample with straight surface to show that the model performs as expected. The SAW is generated by ten double electrode finger pairs. Each of the electrodes has a width equal to 0.7 μm and is placed 0.7 μm apart such that the wavelength of the generated SAW is 5.6 μm. GaAs is a piezoelectric material with cubic crystal structure. The material constants used in the piezoelectric model are given in Tables I and II and are here given in the usual matrix form for compactness reasons. The frequency is $f_{\text{SAW}} = 510$ MHz (where $f_{\text{SAW}} = \omega_{\text{SAW}} / 2\pi$) and the applied electric potential is $V_p = 1$ V. The constant σ_j controlling the damping in the PMLs is set to 10^{10}. GaAs is piezoelectric in the [110] direction, so for the SAW to propagate in this direction the material tensors have to be rotated by the angle $\varphi_2 = \pi/4$. Second order Lagrange elements are used for all the calculations. In Fig. 2(a) the displacement u_2 in the x_2-direction is plotted in the domain with a displacment scaling factor set to 1000, and it is seen that the SAW is generated at the electrodes and propagates away from them to the right and the left. In the PMLs the wave is gradually absorbed. The same results are illustrated at Fig. 2(b) where the absolute amplitude abs(u_2) is plotted along the material surface. It is seen how a standing wave is generated at the electrodes because the SAW here travels in both directions. Away from the electrodes the SAW is a traveling wave and therefore the amplitude is nearly constant. It is also seen how the SAW is absorbed in the PMLs. In Fig. 3(a) the displacements u_1 and u_2 are plotted as function of the depth for $x_1 = 85$ μm. It is seen that the displacements are concentrated within one SAW wavelength of the surface as expected. Below the surface they have smaller oscillations. This is due to the finite depth and the use of the PMLs that are not exactly acting as an infinite domain. On Fig. 3(b) the absolute amplitude abs(u_2) normalized with the square root of the applied electric power P is plotted as function of the frequency f_{SAW} at a point on the surface to the right of the

TABLE II. The piezoelectric stress constants and the permittivity constants for the materials used in the piezoelectric model.

Material	e_{14} (C m^{-2})	e_{15} (C m^{-2})	e_{24} (C m^{-2})	e_{25} (C m^{-2})	e_{31} (C m^{-2})	e_{32} (C m^{-2})	e_{33} (C m^{-2})	e_{36} (C m^{-2})	ε_{11}^S (10^{-11} F m)	ε_{22}^S (10^{-11} F m)	ε_{33}^S (10^{-11} F m)
GaAs	−0.160	0	0	−0.160	0	0	0	−0.160	9.735	9.735	9.735
Si	0	0	0	0	0	0	0	0	11.5	11.5	11.5
SiO_2	0	0	0	0	0	0	0	0	2.37	2.37	2.37
ZnO	0	−0.480	−0.480	0	−0.573	−0.573	1.321	0	7.38	7.38	7.83

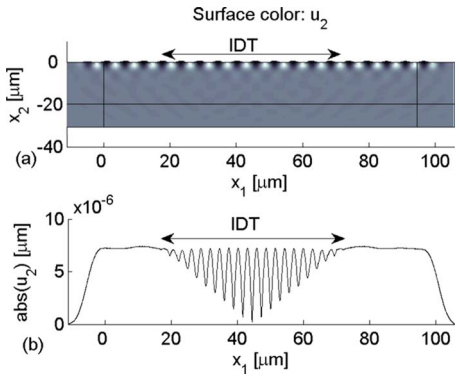

FIG. 2. (Color online) Generation of a SAW in a GaAs sample by the piezoelectric model. The position of the IDT is indicated. (a) The color indicates the displacement u_2 and the shape of the surface is deformed with the unified displacements u_1 and u_2. (b) The graph shows the absolute amplitude abs(u_2) along the material surface as function of x_1

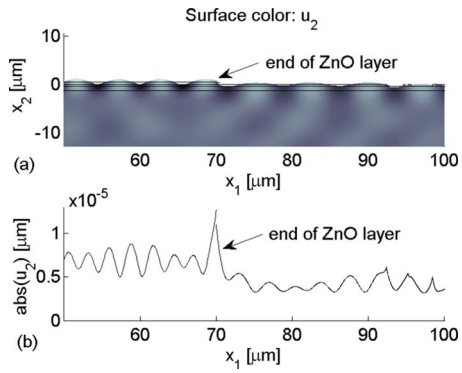

FIG. 4. (Color online) Generation of SAWs in a SOI sample by the piezoelectric model. The results are given to the right of the IDT. (a) The color indicates the displacement u_2 and the shape of the surface is deformed with the unified displacements u_1 and u_2. (b) The graph shows the absolute amplitude abs(u_2) along the material surface as function of x_1.

IDT for the frequency interval of 210–810 MHz for 10 and 20 electrode pairs, respectively. The power P is calculated by the expression[16]

$$P = \Re \int_{L_{\mathrm{el}}} \frac{V(i\omega D_2 m_2)^*}{2} dL, \tag{25}$$

where L_{el} corresponds to boundaries with the electrodes and m_2 is the normal vector to the upper surface. Figure 3(b) shows that the highest value of abs(u_2)/$\sqrt{P}$ appears at f_{SAW} =510 MHz, which corresponds to the frequency found by experiments for a GaAs sample, see Ref. 18. Hence, these results show that the piezoelectric model performs as expected for generation of SAWs. It can also be observed from Fig. 3(b) that when the number of electrode pairs increases, the bandwidth decreases as more of the applied energy is confined to the SAW and consequently the amplitude increases. For twice as many fingers the bandwidth is halved, which is expected as the bandwidth is inversely proportional to the number of finger pairs (see Ref. 15). In practical constructions several hundred finger pairs are used in order to generate a strong SAW. For computational reasons only a fraction of the finger pairs can be used in these calculations. This means that a SAW with a smaller amplitude as in practice is used and the acousto-optical interaction is therefore also smaller than in experiments. However, the same physical effects are expected, which is discussed further in Sec. III C 1.

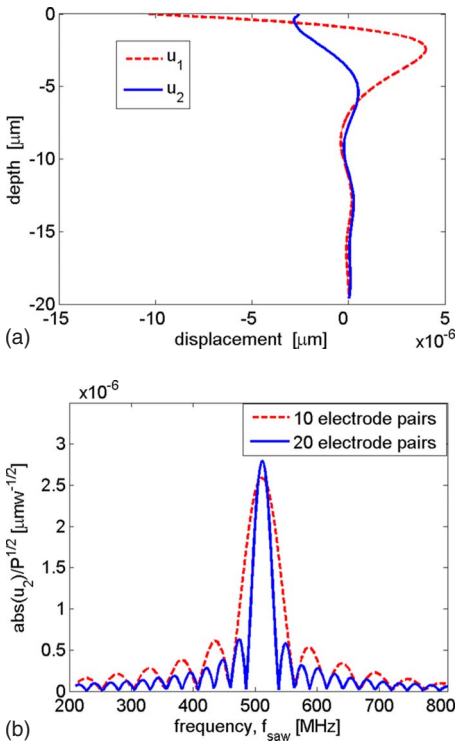

FIG. 3. (Color online) Results for the SAW in the GaAs substrate. (a) Displacements u_1 and u_2 as function of depth at position x_1=85 μm. (b) The absolute amplitude abs(u_2) normalized with the square root of the electrical power P as function of the frequency f_{saw} for 10 and 20 electrode pairs.

In Refs. 8 and 9 results for the acousto-optical modulation in a MZI with GaAs waveguides on a $Al_{0.2}Ga_{0.8}As$ layer were presented as well as results for a MZI with Si waveguides on a SiO_2 layer. In the first case a relative modulation of 40% was obtained with straight waveguides, but for the SOI sample the modulation was only between 0% and 8%. In this work attention is given to the SOI sample in order to understand the unsatisfactory performance and what can be done to improve the modulation. As Si is not piezoelectric the SAW is generated in a ZnO layer on top of the Si from which the SAW propagates toward the rest of the sample with the optical waveguides. The geometry is indicated on Fig. 1(b). The IDT consists of double double finger electrode pairs where each of the electrodes again has a width of 0.7 μm such that the wavelength of the generated SAW is 5.6 μm. The material constants for Si, SiO_2, and ZnO used in the piezoelectric model are given in Tables I and II. The applied potential is V_p=1 V and it is driven with the frequency f_{SAW}=630 MHz. After numerical experiments the constant σ_j in the PMLs is set to 10^{10}. All the materials are rotated with $\varphi_2=\pi/4$ such that the SAW propagates along the [110] direction. In Fig. 4(a) a zoom of the displacements u_2 around the end of the ZnO layer is plotted and it is seen how the wave is generated at the electrodes to the left and propagates from the ZnO layer to the rest of the sample with the waveguides to the right. In Fig. 4(b) the absolute ampli-

TABLE III. Stress-optical constants (Ref. 19).

Material	n_0 (-)	C_{11}, C_{22}, C_{33} (10^{-12} Pa^{-1})	C_{12}, C_{13}, C_{23} (10^{-12} Pa^{-1})	C_{44}, C_{55}, C_{66} (10^{-12} Pa^{-1})
Si	3.42	−11.35	3.65	0
SiO_2	1.46	0.65	4.50	−3.85

tude abs(u_2) is plotted along the material surface. From the two figures it is seen that there is a decrease in amplitude when the SAW propagates out in the Si/SiO_2 layer. In the ZnO layer the amplitude has a magnitude of around 0.8×10^{-5} μm. In the Si/SiO_2 layer the amplitude is almost halved and has a size around 0.5×10^{-5} μm—only 60% of the amplitude in the ZnO. So the SAW looses energy because of reflections and a change in material with different impedances. It is noted that smaller oscillations in the amplitude occur, and these indicate that standing waves appear in the device due to reflections from the discontinuity of the surface. Another reason for the poor modulation is that the wavelength of the SAW is 5.6 μm in the ZnO layer as expected from the size of the electrodes. However, when the SAW continuous to the Si/SiO_2 layer, the amplitude drops and the wavelength increases to approximately 7.3 μm—an increase of approximately 30%. This means that the two waveguides are no longer placed a multiple of half wavelengths apart, so to obtain a better modulation this distance must be corrected. To improve the model further it is necessary to examine how the SAW interacts with the optical wave in the waveguides, so the coupled acousto-optical model must be used.

B. Simulation of optical waves

In this section results for the optical eigenvalue problem are presented for the SOI MZI when x_4 from Fig. 1(b) is corrected to 4.94 μm such that there are 1.5 SAW wavelengths between the center of the waveguides. The free space wavelength of the optical wave is set to $\lambda_0 = 1531$ nm. The material constants for Si and SiO_2 used in the optical model are given in Table III. For air simply the refractive index $n_0 = 1$ is used. The size of the optical calculation domain is 5×4 μm. Figure 5 shows the x_3-component of the time averaged power flow of the fundamental mode in the waveguides when no stresses are applied. From the two graphs that the biggest difference in effective refractive index $(n^l_{\text{eff},0} - n^r_{\text{eff},0})/\sqrt{P}$ between the left and the right waveguide is at the expected positions of the SAW with the value of 2.00×10^{-6} $W^{-1/2}$. It is also observed that there are losses between the waveguides due to reflections as $\Delta n_{\text{eff},0}/\sqrt{P}$ in the right waveguide never reaches the extreme values achieved in the left waveguide. Again, it is emphasized that the values of $\Delta n_{\text{eff},0}/\sqrt{P}$ are small, which is due to the limited numbers of electrodes used.

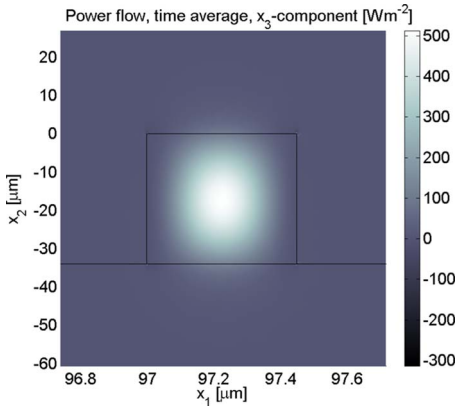

FIG. 5. (Color online) The x_3-component of the time averaged power flow of the fundamental mode in the waveguides when no stresses are applied.

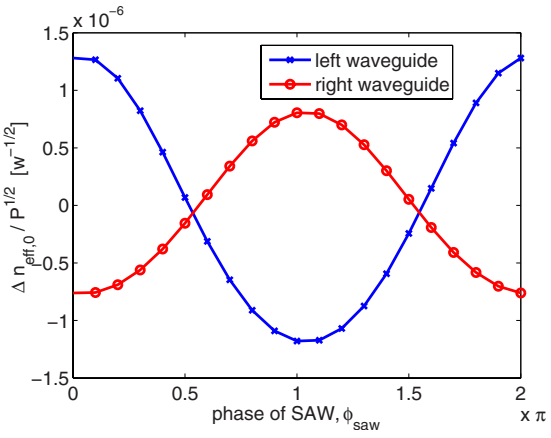

FIG. 6. (Color online) Change in the effective refractive index $n_{\text{eff},0}/\sqrt{P}$ of the fundamental mode in the two waveguides normalized by the square root of the power P as function of the SAW phase ϕ_{SAW}. $\phi_{\text{SAW}} = 0$ corresponds to a wave crest in the left waveguide and a trough in the right.

C. Increasing the difference in effective refractive index between the waveguides

In this subsection suggestions on how to change the geometry in order to increase the difference in effective refractive index $n_{\text{eff},0}$ between the waveguides are presented. An increased difference will improve the light modulation.

1. Changing the waveguide size

In this study the height and the width of the waveguides are changed. Figure 7(a) shows the difference in effective refractive index $(n^l_{\text{eff},0} - n^r_{\text{eff},0})/\sqrt{P}$ as function of the height h when a wave crest appears at the left waveguide and a trough at the right waveguide. The calculations are done for both the original case with six electrode pairs and for 12 electrode pairs. It is observed that there is an optimal height of the

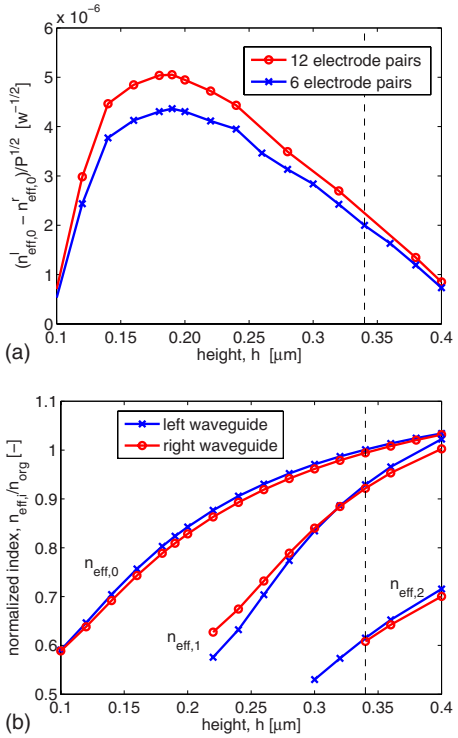

FIG. 7. (Color online) Results for a study of the height h of the waveguides with (- - -) indicating the results for the original waveguide geometry. (a) Difference in effective refractive index $(n^l_{\mathrm{eff},0}-n^r_{\mathrm{eff},0})/\sqrt{P}$ of the fundamental mode between the two waveguides as function of h for 6 and 12 electrode pairs. (b) The effective refractive index $n_{\mathrm{eff},i}$ for the three lowest order modes in the waveguides normalized to the value $n_{\mathrm{eff,org}}$ of the fundamental mode in the left waveguide for the original geometry as functions of h.

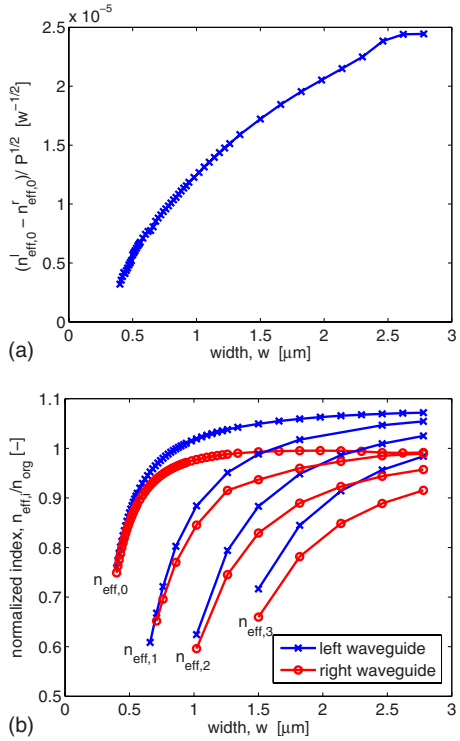

FIG. 8. (Color online) Results for a study of the waveguide width w for the optimal height h=0.19 μm. (a) Difference in effective refractive index $(n^l_{\mathrm{eff},0}-n^r_{\mathrm{eff},0})/\sqrt{P}$ of the fundamental mode between the two waveguides as function of w. (b) The effective refractive index $n_{\mathrm{eff},i}$ for the four lowest order modes in the waveguides normalized to the value $n_{\mathrm{eff,org}}$ of the fundamental mode in the left waveguide for the original geometry as functions of w.

waveguides for which the biggest difference in $n_{\mathrm{eff},0}$ is obtained. The optimal height is for both 6 and 12 electrode pairs found to be 0.19 μm with a difference in index equal to 4.36×10^{-6} $\mathrm{W}^{-1/2}$ for 6 electrode pairs, 2.2 times bigger than for the original height. The reason for this optimum is first of all that when the height of the waveguides decreases the reflections of the SAW due to the interruptions at the surface will be reduced and the stresses in the waveguides will be bigger. With a smaller height the center of the optical wave will move closer to the SiO_2 surface and will experience larger stresses as the biggest stresses of a SAW are found just below the surface of the material and not at the surface, see Fig. 3(a). However, when the height is too small, the optical wave will be less confined in the waveguide and will be increasingly influenced by the SiO_2 and the air. The air will for obvious reasons not contribute to an index difference in the two waveguides and the SiO_2 will have a negative influence on the difference. This is seen from the signs of the stress-optical constants. For Si the stress-optical constant with the biggest numerical value has a negative sign and therefore the refractive index will mainly increase for positive stresses. For SiO_2 C_{11}, C_{12}, C_{13} C_{22}, C_{23}, and C_{33}, which will relate to the normal stresses, all have a positive sign and here the refractive index will mainly decrease for positive stresses. So, if a big part of the optical wave propagates in the air and the SiO_2, the difference between the effective refractive indices will decrease. The graph on Fig. 7(a) therefore shows an optimal height of the waveguides, which is a solution of a nontrivial interaction of how much the SAW is reflected and how close the center of the optical wave can get to the SiO_2 surface and still be well confined in the waveguide. The fact that the same optimal height is found for both 6 and 12 electrode pairs indicates that the design conclusions are independent of the number of electrode pairs. An increase in electrodes will just increase the difference in $n_{\mathrm{eff},0}$, which is expected as more of the applied energy will be confined to the SAW. Figure 7(b) shows the effective refractive index for the zero, first, and second order mode normalized to the value $n_{\mathrm{eff,org}}$ of the fundamental mode in the left waveguide for the original height as functions of h. $n_{\mathrm{eff},i}$ are in all cases decreasing for decreasing height as less Si, with high refractive index, is used. The waveguide with the original height supports the three lowest order modes, whereas for the optimal height the waveguide is single moded.

A study of the width of the waveguide is then done with the height fixed to the optimal height h=0.19 μm and the difference in index between the two waveguides is seen on Fig. 8(a). The difference in $n_{\mathrm{eff},0}$ increases with increasing w. This can be explained by observing how the mode changes. When w is increasing the confined optical mode will also increase in the horizontal direction. This means that the mode will experience more stresses as long as w is smaller than half a SAW wavelength. At the same time the mode is also getting less confined to the waveguide, meaning that it will be more influenced by the surrounding materials, which

will have a negative influence on the index change as discussed above. However, this effect is smaller than the positive effect from the increased stresses in the waveguide. The limit for the increase is when w approaches half a SAW wavelength, where the change in $n_{\text{eff},0}$ slowly stops to increase. However, before that the mode in the right waveguide with the SAW trough will start to degenerate into two modes, so the graph is therefore stopped there. The difference in index is now 2.44×10^{-5} $\text{W}^{-1/2}$, which is more than 12 times bigger than for the original waveguide geometry. However, when w is increasing the waveguides will start to be multimoded again as seen on Fig. 8(b). Here $n_{\text{eff},i}/n_{\text{org}}$ for the first four lowest order modes in the two waveguides are shown as functions of w. The waveguide is single moded until $w=0.64$ μm and the difference in index is here 7.76×10^{-6} $\text{W}^{-1/2}$, which is almost four times bigger than for the original waveguide geometry. This shows that it is possible to improve the optical modulation by changing the waveguide size such that the mode is moved closer to the surface and extended in the width to experience more stresses.

It is noted that even though the optimal height found is optimal for the original width, it is not certain that this height is optimal when the width is changed afterwards. As the optical modes change when the waveguide geometry is varied, it is not straightforward to apply a systematic optimization algorithm. Instead an extended parameter study has to be performed in order to find the height and width that are optimal together. This, however, is beyond the scope of the paper.

2. Other device structures

Alternative to changing the size of the waveguides, other device structures can be thought of to improve the acousto-optical modulation. As the stresses from the SAW have their maximum just below the surface, it is expected that the acousto-optical interaction is increased if the waveguides are buried in the SiO_2 layer instead of being placed above the layer. A calculation is carried out with the original waveguide size, but with the waveguides placed such that their upper surface is leveled with the substrate surface. The difference in effective refractive index is 2.14×10^{-5} $\text{W}^{-1/2}$, which is more than ten times bigger than for the original waveguides on top of the surface. So with buried waveguides it is possible to improve the modulation drastically.

Another idea is to use an IDT at each side of the MZI arms. The two SAWs will be reflected back toward the waveguides when reaching the opposite IDT and a standing wave pattern will appear, which is expected to have enhanced amplitude compared to the original traveling wave. The distance between the two IDTs is tuned such that the standing wave achieves its maximum amplitude. The waveguides have the original size and eight electrode pairs are used in each IDT. The difference in effective refractive index is calculated for the case with the electric potential applied at one IDT for double fingers, the potential applied at both IDTs for double and single fingers and the results are scaled by the squared applied power, see Table IV. It is seen that the difference in effective refractive index is increased when two IDTs are used, as expected, and that the difference in index is more than 1.5 times bigger than for one IDT when using double fingers. The effect is small, but is expected to be bigger when more electrodes are used.

TABLE IV. Results for the difference in effective refractive index $(n^l_{\text{eff},0}-n^r_{\text{eff},0})/\sqrt{P}$ for different combinations of IDT numbers and single and double electrode fingers, $(\text{W}^{-1/2})$.

	1 IDT (double fingers)	2 IDTs (double fingers)	2 IDTs (single fingers)
$\frac{n^l_{\text{eff},0}-n^r_{\text{eff},0}}{\sqrt{P}}$	1.93×10^{-6}	3.04×10^{-6}	2.34×10^{-6}

IV. CONCLUSION

This work presents a general finite element method to calculate the acousto-optical interaction between a SAW and optical waves in waveguides in a finite device.

The SAW is generated by an IDT using a piezoelectric model for an inhomogeneous material implemented in the high-level programming language COMSOL MULTIPHYSICS, where reflections from the boundaries are avoided by PMLs. Results of the SAW generation in a GaAs sample are presented, which show that the model works satisfactory as SAWs are generated at the electrodes and are absorbed in the PMLs. The frequency, which gives the biggest amplitude, is found to be the same as in experiments.

This model is then coupled to a model of the optical waves in the waveguides of a SOI MZI where the optical modes are found by solving the time-harmonic wave equation. By applying stresses from a SAW, it is shown that the effective refractive index of the fundamental optical mode has its maximum value for a SAW crest and minimum value for a SAW trough, as is expected.

This coupled finite element model is then employed to study geometry changes in the SOI MZI in order to increase the difference in effective refractive index in the two waveguide arms such that the optical modulation in the device is improved. A study of the height of the waveguides shows that an optimal height exists for the device, which is a result of a nontrivial compromise of how much the SAW is reflected, because of the interrupted surface, and how close the center of the optical wave can get to the SiO_2 surface and still be well confined in the waveguide. The difference in effective refractive index is approximately 2.2 times bigger for the optimal height and the waveguides have become single moded. The same optimal height is found when the number of electrode pairs in the IDT is doubled and this indicates that the design results in this work are independent of the number of electrode pairs. The width of the waveguides is then studied for the optimal height. The difference in effective refractive index increases for increasing width as the optical mode is influenced by increasing stresses from the SAW until the width reaches half a SAW wavelength. The difference in effective refractive index is 12 times bigger than for the original geometry, and if the waveguide has to stay single moded the difference is approximately four times bigger. The stresses of the SAW have their maximum just below the surface and a calculation where the

waveguides with the original size are buried below the surface shows that the difference in effective refractive index can be increased more than ten times by this change. Finally, it is tested if a standing wave created by two IDTs can improve the interaction. When double finger electrodes are used the difference in effective refractive index is 1.5 times bigger than the original case, and for single fingers it is 1.2 times bigger.

Further work includes a study of other geometry parameters as the height of the different layers as well as employing an optimization method as topology optimization (see Refs. 20 and 21) to improve certain parts of the geometry such as the shape of the waveguides and structures in between them.

ACKNOWLEDGMENTS

This work is supported by the European FP6 research project ePIXnet—*European Network of Excellence on Photonic Integrated Components and Circuits*. The authors thank the partners from the joint research group of ePIXnet *Photonic Switches and Modulators based on Surface Acoustic Waves* Paulo V. Santos and Markus Beck from Paul-Drude-Institut für Festkörperelektronik, Berlin, Germany and Mike van der Poel from Department of Photonics Engineering, Technical University of Denmark, for valuable input related to the model presented.

The authors are grateful to Jakob S. Jensen from the Department of Mechanical Engineering and Martin P. Bendsøe from the Department of Mathematics, Technical University of Denmark, for helpful discussions related to the presented work.

The support from Euro-horcs/ESF European Young Investigator Award (EURYI) through the grant *Synthesis and Topology Optimization of Optomechanical Systems* as well as from the Danish Center for Scientific Computing (DCSC) is gratefully acknowledged.

[1] K.-Y. Hashimoto, *Surface Acoustic Wave Devices in Telecommunications, Modeling and Simulation* (Springer, Berlin, 2000).
[2] R. M. White and F. W. Voltmer, Appl. Phys. Lett. **7**, 314 (1965).
[3] S. Takahashi, H. Hirano, T. Kodama, F. Miyashiro, B. Suzuki, A. Onoe, T. Adachi, and K. Fujinuma, IEEE Trans. Consum. Electron. **CE-24**, 337 (1978).
[4] Proceedings of the International Symposium on Surface Acoustic Wave Devices for Mobile Communication, 1992, edited by K. Shibayama and K. Fujinuma (unpublished).
[5] U. Wolff, F. L. Dickert, G. K. Fischauer, W. Greibl, and C. C. W. Ruppel, IEEE Sens. J. **1**(1), 4 (2001).
[6] C. Gorecki, F. Chollet, E. Bonnotte, and H. Kawakatsu, Opt. Lett. **22**, 1784 (1997).
[7] M. M. de Lima, Jr., and P. V. Santos, Rep. Prog. Phys. **68**, 1639 (2005).
[8] M. M. de Lima, Jr., M. Beck, R. Hey, and P. V. Santos, Appl. Phys. Lett. **89**, 121104 (2006).
[9] M. van der Poel, M. Beck, M. B. Dühring, M. M. de Lima, Jr., L. H. Frandsen, C. Peucheret, O. Sigmund, U. Jahn, J. M. Hwam, and P. V. Santos, Proceedings of European Conference on Integrated Optics and Technical Exhibition, Copenhagen, Denmark, 25–27 April 2007 (unpublished).
[10] S. Ballandras, M. Wilm, P.-F. Edora, A. Soufyana, V. Laude, W. Steichen, and R. Lardat, J. Appl. Phys. **93**, 702 (2003).
[11] D. B. Carstensen, T. A. Christensen, and M. Willatzen, Proceedings of the Nordic COMSOL Conference, Denmark, 2006 (unpublished).
[12] J. Wang and J. Lin, J. Intell. Mater. Syst. Struct. **16**, 623 (2005).
[13] U. Basu and A. Chopra, Comput. Methods Appl. Mech. Eng. **192**, 1337 (2003).
[14] COMSOL Reference Manual for COMSOL 3.3A, COMSOL AB, Stockholm, www.comsol.se.
[15] D. Royer and E. Dieulesaint, *Elastic Waves in Solids I*, 1st ed. (Springer, New York, 2000).
[16] B. A. Auld, *Acoustic Fields and Waves in Solids, Volume I*, 1st ed. (Wiley, New York, 1973).
[17] R. Syms and J. Cozens, *Optical Guided Waves and Devices*, 1st ed. (McGraw-Hill, New York, 1992).
[18] M. M. de Lima, Jr., F. Alsina, W. Seidel, and P. V. Santos, J. Appl. Phys. **94**, 7848 (2003).
[19] M. Huang, Int. J. Solids Struct. **40**, 1615 (2003).
[20] M. P. Bendsøe and O. Sigmund, *Topology Optimization, Theory, Methods and Applications* (Springer-Verlag, Berlin, 2003).
[21] J. S. Jensen and O. Sigmund, Appl. Phys. Lett. **84**, 2022 (2004).